Separation of intrinsic absorption and scattering attenuation from Lg coda decay in central France using acoustic radiative transfer theory

Céline Lacombe, Michel Campillo, Anne Paul, Ludovic Margerin

Geophys. J. Int. (2003) **154,** 417–425

Separation of intrinsic absorption and scattering attenuation from *Lg* coda decay in central France using acoustic radiative transfer theory

Céline Lacombe, Michel Campillo, Anne Paul and Ludovic Margerin

Laboratoire de Géophysique Interne et Tectonophysique, Observatoire de Grenoble, Université Joseph Fourier and CNRS, BP 53X, 38041 *Grenoble Cedex, France. E-mail: apaul@obs.ujf-grenoble.fr*

Accepted 2003 January 27. Received 2003 January 17; in original form 2002 March 7

SUMMARY

Radiative transfer theory is applied to the measurement of average values of the transport mean free path and absorption length (l_a, related to the intrinsic quality factor) in the lithosphere beneath France by comparing simulated and observed coda envelopes of regional records. The lithosphere is modelled as a flat layer representing the crust overlying a half-space representing the mantle, with different velocities and scattering properties. We infer the average values of l_a (assumed to be constant over the whole medium) and transport mean free paths in the crust (l_c^*) and mantle (l_m^*) by minimizing a misfit function between observed and modelled *Lg* coda envelopes. This comparison is conducted in two different time windows, the whole *Lg* coda (group velocity smaller than 2.6 km s^{-1}) and the early coda ($v_g < 2.6$ km s^{-1} and lapse time smaller than 300 s), when coda envelopes have decay rates that depend on distance. In the early coda, a single set of parameters l_a and l_c^* minimizes the misfit function. Using the whole *Lg* coda time window, we find that many models fit the data equally well. We explain this difference by the common decay rate of envelopes independent of distance over most of the coda window. The measurement of the attenuation of the coherent *Lg* wave complements these results to constrain l_a and l_c^*. We find that a model with $l_c^* \sim 250$ km and $l_a \sim 150$ km explains the attenuation of both the direct *Lg* wave train and the entire *Lg* coda with both time and distance at 3 Hz. However, the trade-off between the two parameters is too strong to conclude reliably on the dominance of intrinsic on scattering attenuation.

Key words: attenuation, crustal structure, seismic waves, scattering.

INTRODUCTION

Following the work of Aki (1969) and Aki & Chouet (1975), the hypothesis that the coda of seismic records is made of waves scattered on heterogeneities randomly distributed in the lithosphere has become widely accepted. To evaluate statistical properties of this heterogeneity, seismologists have tried to evaluate the relative amount of attenuation due to scattering and intrinsic absorption.

Heterogeneity in the crust is observed on a broad range of scales (Sato & Fehler 1998; Wu & Aki 1988a) and its influence on wave propagation cannot be investigated using deterministic approaches. Considering the lithosphere as a random medium, the average intensity of scattered waves is governed by a transport equation (Chandrasekhar 1960), which was rigorously derived from the acoustic wave equation by Ryzhik *et al.* (1996). The scalar radiative transfer equation has been applied to describe wave propagation in the lithosphere by, for example, Wu (1985), Wu & Aki (1988b), Hoshiba (1991, 1994, 1997), Sato *et al.* (1997) Margerin *et al.* (1998) and Zeng *et al.* (1991). The heterogeneity of a multiple-scattering medium is described by two parameters, the scattering mean free path l and the transport mean free path l^*. l is the characteristic length of extinction and l^* is the propagation distance above which the wave front loses memory of its initial propagation direction. In this paper and for the sake of simplicity, we assume that scattering is isotropic and thus that $l = l^*$. We also define a Q-factor associated with scattering (Q_{scat}) as $Q_{scat} = 2\pi f l^*/v$, where f denotes the frequency and v the group velocity. The Q-factor associated with intrinsic attenuation (Q_{int}) is also related to an absorption length l_a defined as $l_a = Q_{int} v/2\pi f$.

Wu (1985) was the first to take multiple scattering into account to measure the relative contributions of scattering and intrinsic absorption to total attenuation. His method is based on the radiative transfer theory, which gives a theoretical model of energy propagation in a randomly heterogeneous elastic medium. It assumes that the lithosphere is a uniform half-space (no variation of heterogeneity or wave velocity with depth). Fehler *et al.* (1992) proposed a revised method of Wu's technique still assuming a uniform half-space, which is called the 'multiple lapse time window analysis' (MLTWA). Many studies have been carried out in different regions using this method (see, for example, Mayeda *et al.* (1992) for Q_{int} and Q_{scat} separation in Hawaii, Long Valley and Central California, Hoshiba (1993) in Japan, Mayeda *et al.* (1991) and

Jin *et al.* (1994) in Southern California or Ugalde *et al.* (1998) for Northern Venezuela).

The assumption of a uniform distribution of scatterers in the lithosphere is probably unrealistic, as emphasized for example by Abubakirov & Gusev (1990), Hoshiba (1994) and Gusev (1995). First, the velocity contrast at the crust–mantle transition must be taken into account. Moreover, deep seismic soundings (which give a description of the heterogeneity of the lithosphere) often reveal strong variations of the seismic reflectivity at a depth corresponding to the Moho (see, for example, Bois *et al.* (1988) for seismic soundings in France or Fuchs *et al.* (1987) for deep reflection experiments in Germany). Thus, both depth-dependent velocity and scattering properties must be included in models of the lithosphere. Margerin *et al.* (1999) used such models to evaluate the crustal mean free path and the intrinsic Q factor in Mexico. Using records of local earthquakes at epicentral distances smaller than 50 km, they showed that a model consisting of a highly heterogeneous crust overlying a transparent mantle explains the observed coda $Q(Q_c)$. They also concluded that a large $Q_{\rm int}^{-1}$ (strong intrinsic absorption) is not required to explain the observed Q_c in Mexico. More recently, Hoshiba *et al.* (2001) measured intrinsic absorption and scattering attenuation in northern Chile using the multiple lapse time window analysis and assuming depth-dependent velocity structure and mean free path. Using events recorded at hypocentral distances smaller than 160 km, they concluded that the crustal mean free path is $\simeq$300 km and the absorption length $\simeq$100 km at 3 Hz. Note that Margerin *et al.* (1999) and Hoshiba *et al.* (2001) did not use the same part of the coda time window. While Margerin *et al.* (1999) used the late coda when all records exhibit a steady decay independent of epicentral distance, Hoshiba *et al.* (2001) focused on the first part of the coda when the energy decay depends on distance.

The goal of this study is to find a model that explains the energy decay with time and distance of the whole *Lg* coda as well as the attenuation properties of direct waves. We use regional records at epicentral distances between 100 and 900 km, covering a much broader range than the data used by Margerin *et al.* (1999) and Hoshiba *et al.* (2001). These regional records are dominated by a clear *Lg* wave train, which is made of the superposition of *S* waves supercritically reflected and trapped in the crust. Since *Lg* waves sample the entire crust, parameters measured from this phase can be regarded as average values for the whole crust. To obtain average values of transport mean free path and intrinsic Q in the lithosphere, we compare the decay rate of *Lg* coda with both time and distance to the results of numerical simulations computed for models with depth-dependent scattering properties and velocity. The best set of parameters is estimated by minimizing a misfit function between modelled and observed *Lg* coda energy envelopes. To further constrain our model using the attenuation characteristics of the direct *Lg* wave, we use the results obtained in the same region by Campillo *et al.* (1985) and Campillo & Plantet (1991).

OBSERVATIONS

Our data set is made of records of the two largest-magnitude earthquakes ($m_b = 5.3$ and 5.1) that occurred in France between 1996 and 2001. The first one occurred on 1996 July 15 in Annecy (45.93°N–6.09°E) at 2 km depth. The second one was located near Saint-Gaudens (42.92°N–0.60°E) at 10 km depth on 1999 October 4. Both event locations are shown as circles in Fig. 1. Seismograms were recorded by the LDG/CEA short-period network, which covers most of the country (Nicolas *et al.* 1982). The locations of the 30 stations that recorded at least one of the two events are shown as

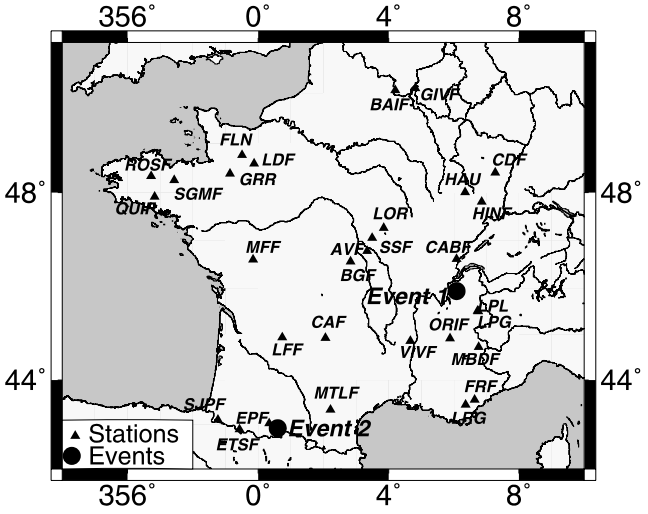

Figure 1. Location map of earthquakes and stations used in this study.

triangles in Fig. 1. Fig. 2 shows an example of vertical-component seismograms (filtered between 1 and 5 Hz) of the Saint-Gaudens earthquake for epicentral distances between 139 and 860 km. The *Lg* wave train is clearly the dominant phase of the seismograms. For such epicentral distances, waves travel across different geological structures. However, they do not cross the Alpine and Pyrenean mountain ranges where *Lg* extinction is observed (see Campillo *et al.* 1993) for the Ivrea body extinction in the Alps, and Chazalon *et al.* (1993) for the Western Pyrenean extinction). Apart from these two mountain belts, the Variscan platform crust of central France is fairly laterally homogeneous and we can reasonably assume that regional phases travel across a 1-D lithosphere with laterally homogeneous statistical properties.

Energy envelopes recorded at all stations for the Saint-Gaudens earthquake are plotted in Fig. 3 after bandpass filtering around 3 Hz. This figure documents three different regimes in the decay of energy with time. After the arrival of direct waves and at times smaller than 300 s, energy curves display different decay rates at different epicentral distances. This property is used in the so-called multiple lapse time window analysis to separate $Q_{\rm int}$ from $Q_{\rm scat}$ (e.g. Hoshiba 1993). It characterizes the multiple-scattering regime and the energy decay can be explained with the radiative transfer theory (Rytov *et al.* 1989). In the 300–500 s time window, all energy curves merge and exhibit a steady decay independent of distance, which is characteristic of the so-called diffusion regime. Diffusion occurs after a sufficiently large number of scattering events. As each scattering event distributes energy in all directions of space, the distribution of energy is very close to being isotropic after a large number of scattering events (Kourganoff 1963). In this regime, the wave energy is governed by a diffusion equation. At large times, its solution exhibits an asymptotic behaviour and energy becomes independent of distance.

DATA PROCESSING

Seismograms were filtered in three narrow frequency bands centred on 2, 3 and 5 Hz, with bandwidths of 0.66, 1 and 1.65 Hz, respectively ($\Delta f/f = 0.33$). Amplitudes were then squared to obtain the coda energy envelope. The background noise preceding the first arrivals was processed in a similar way to determine the time when the signal-to-noise ratio becomes smaller than 4.

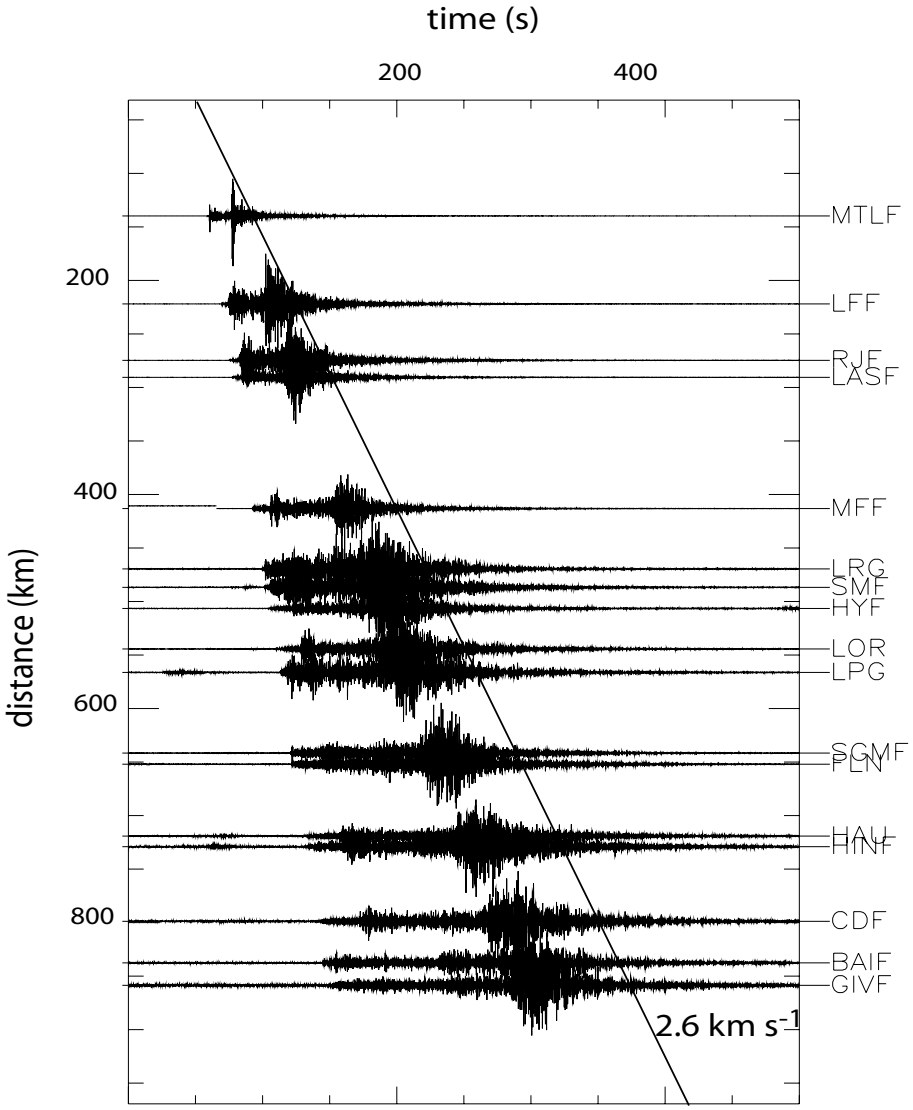

Figure 2. Vertical-component seismograms recorded for the Saint-Gaudens earthquake at different epicentral distances and filtered between 1 and 5 Hz.

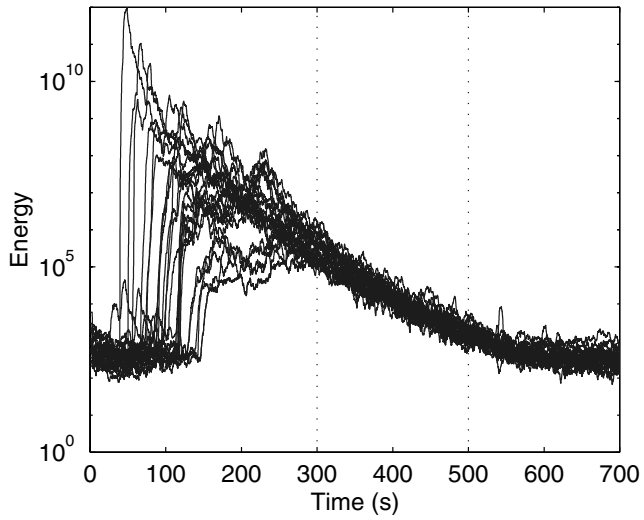

Figure 3. Envelopes of all seismograms recorded for the Saint-Gaudens earthquake after filtering around 3 Hz. The vertical dotted lines delimit the time interval when all decay curves merge independent of epicentral distance.

The energy of the coda recorded at a given station is affected by the local site amplification in addition to the influence of the propagation medium. All measured energies have thus to be corrected for site and source effects. The correction is based on the separability of source, site and path effects (Aki 1980). The main assumption is that, at large times and without a site effect, the energy level is the same at all stations. This is true if we assume that at large lapse times, waves propagate in the diffusion regime and energy is almost uniformly distributed in space. The validity of the diffusion assumption will be discussed later.

The site amplifications at most stations were computed from direct *Lg* amplitudes by Campillo *et al.* (1985) who used station FLN as a reference site. We also assume that the site amplification factor at FLN is equal to 1. Since path and source terms become independent of the station when t is large, the energy ratio between two seismograms at a given frequency in a given time window equals the ratio between the local site amplifications at those stations. We can thus determine the site amplification of each site relative to FLN. This was achieved in 50 s wide time windows centred at a lapse time of 450 s.

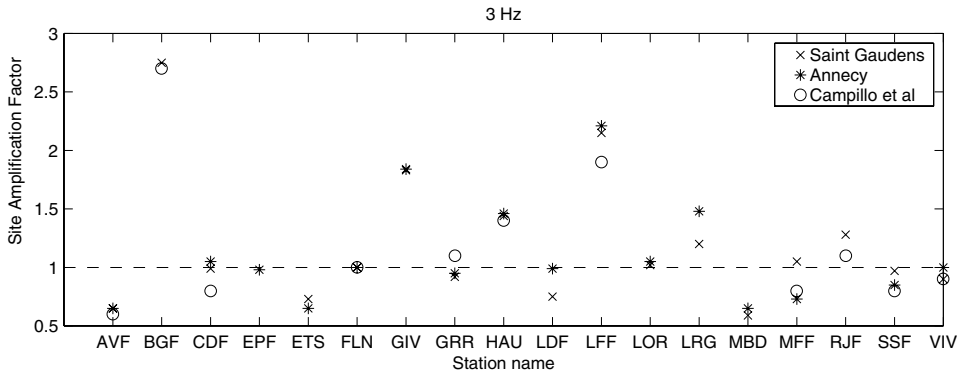

Figure 4. Comparison between the site amplification factors measured by Campillo *et al.* (1985) (○) and those obtained with the Saint-Gaudens (×) and Annecy events (∗).

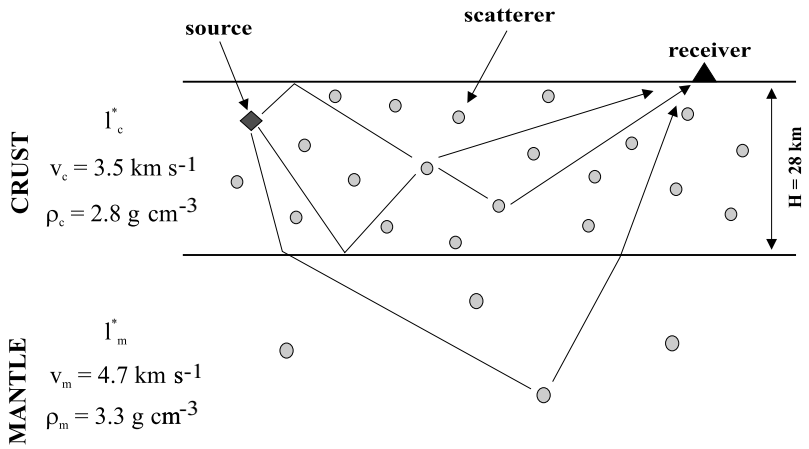

Figure 5. Model used in the simulations.

Fig. 4 shows the values of the site amplification factors measured at 3 Hz for 17 stations using the records of both Annecy (stars) and Saint-Gaudens earthquakes (crosses). They are compared with values obtained at the same stations by Campillo *et al.* (1985) from an inversion of *Lg* amplitude decay with distance for source, site and path effects (circles in Fig. 4). The two methods give very similar results, showing the validity of both the simple site correction method used here and the diffusion assumption.

PARAMETER ESTIMATION

To quantify crust and mantle heterogeneity and intrinsic absorption in France, we compare observed *Lg* coda energy with the results of numerical simulations.

Numerical simulations

Our model includes a flat 28 km thick layer representing the crust overlying a half-space representing the mantle (Fig. 5). The average values of velocities and densities estimated from refraction experiments by Perrier & Ruegg (1973) in central France are given in Table 1. This model assumes that the crust has laterally constant properties and that the intrinsic Q is constant over the whole medium (crust and mantle). The three free parameters are the transport mean free paths of the crust l_c^* and mantle l_m^*, and the absorption length l_a, which we assume for simplicity to be constant over the whole medium. The source is assumed to be isotropic and we consider 37 receivers located at the free surface at epicentral distances corresponding to our data set.

The decay of wave energy with time and distance is modelled using the radiative transfer equation. We assume that no mode conversion occurs (acoustic wave propagation) and that scattering is isotropic. The acoustic radiative transfer equation is solved with Monte Carlo simulations using the procedure described in Lux & Koblinger (1991) and in a number of papers such as Hoshiba (1991) for wave propagation in an infinite space, and Hoshiba (1994, 1997) and Margerin *et al.* (1998) for propagation in a layered medium.

Comparison window and misfit function

Fig. 2 shows that seismograms recorded at regional distance have a long *Lg* coda. As our models only include scattered waves, we

Table 1. Parameters of the model used in the simulations.

	S-wave velocity (km s^{-1})	Density (g cm^{-3})	Q_{int}	Mean free path (km)
Crust	3.5	2.8	200–1500	30–1000
Mantle	4.7	3.3	200–1500	250–100 000

compare simulations with seismograms in time windows when direct waves are negligible. Campillo & Paul (1992) computed *Lg* wave trains in a 1-D stratified model with alternating high- and low-velocity layers in the lower crust. They found that energy can hardly travel at a group velocity smaller than 2.5 km s^{-1}. Dainty & Toksöz (1990) also showed that the long duration of *Lg* coda requires a 3-D scattering process. Considering these results, we compare the observed and simulated energies for group velocities smaller than 2.6 km s^{-1}. We set the end of the time window when the signal-to-noise ratio becomes smaller than 4.

To account for site amplification and source energy, we normalize both observed and simulated energy curves by the average of energy values in the time window [t_0; t_0 + 50 s] with t_0 larger than 300 s (see Fig. 3). We tested that a 50 s wide normalization window is large enough to smooth high-frequency fluctuations in both the data and the Monte Carlo simulations. We considered different values of t_0 between 300 and 450 s and found that it has a negligible influence on the final result.

For a given model, we calculate a misfit function ϵ in half-overlapping moving time windows of duration 40 s:

$$\epsilon = \log \frac{1}{N.M} \sum_{j=1}^{N} \sum_{i=1}^{M} \frac{\left(\left\langle E^{\text{norm}}_{\text{obs}_i}\right\rangle_j - \left\langle E^{\text{norm}}_{\text{simul}_i}\right\rangle_j\right)^2}{\min\left(\left\langle E^{\text{norm}}_{\text{simul}_i}\right\rangle_j^2, \left\langle E^{\text{norm}}_{\text{obs}_i}\right\rangle_j^2\right)}, \quad (1)$$

where log denotes the natural logarithm, N and M are the numbers of stations and moving time windows. $\langle E^{\text{norm}}_{\text{obs}_i}\rangle_j$ and $\langle E^{\text{norm}}_{\text{simul}_i}\rangle_j$ denote the averages of normalized energy for observations and simulations, at station i and in the jth moving time window. min(x, y) denotes the minimum between x and y. This misfit function tends to overweight large values of ($\langle E^{\text{norm}}_{\text{obs}_i}\rangle_j - \langle E^{\text{norm}}_{\text{simul}_i}\rangle_j$). This choice is justified because energy curves are smoothed prior to the estimation of ϵ. Other misfit functions have been tested, which led to very similar final results.

We compare data and simulations for 882 different models where velocities, densities and crustal thickness are held constant while heterogeneity in the crust (l_c^*) and mantle (l_m^*) as well as intrinsic attenuation vary. We consider values of Q_{int} between 200 and 1500 (corresponding to an absorption length l_a between 37 and 278 km at 3 Hz). The crustal transport mean free path (l_c^*) ranges from 30 to 1000 km, and the mantle transport mean free path (l_m^*) varies from 250 to 100 000 km (Table 1). An example of the decay of energy density with time, simulated at an epicentral distance of 220 km, is shown in Fig. 6 for different crustal mean free paths and for a perfectly elastic and transparent mantle ($l_m = \infty$). This figure illustrates how strongly the energy decay depends on the scattering properties of the crust.

RESULTS FOR MODELS WITH A TRANSPARENT MANTLE

In this section, we consider models with a transparent mantle (l_m^* = 100 000 km). The two free parameters are the absorption length in the crust, l_a, and the crustal mean free path, l_c^*. The comparison between data and synthetics is performed in the frequency band 2–4 Hz, which corresponds to the best signal-to-noise ratio.

Whole *Lg* coda time window

Fig. 7 shows maps of the misfit values obtained in a time window including the whole *Lg* coda. Data from both events are considered together. We checked that similar maps are obtained with data from each event considered separately. The grey-scale of the map on the left-hand side of Fig. 7 covers the entire amplitude range of the misfit function while, on the right-hand side, the scale zooms in the narrow amplitude range between the minimum value of ϵ denoted as ϵ_m and ϵ_m + 3 per cent. These maps show that there is no single clear minimum of the misfit function. For example, models with $l_c^* <$ 100 km and $l_a >$ 200 km ($Q_{\text{int}} > 1200$) or with $l_c^* >$ 500 km and $l_a \simeq$ 150 km ($Q_{\text{int}} \simeq$ 800–900) explain the observations equally well although they are very different, showing the trade-off between l_a and l_c^*. In the first one, intrinsic attenuation is negligible and all the observed attenuation can be explained by scattering while in the second one, scattering attenuation is weak and most of the observed attenuation is explained by anelastic absorption. Nevertheless, Fig. 7 shows that l_c^* cannot be smaller than 50 km and l_a than 125 km. The trade-off between l_a and l_c^* is due to the common decay rate documented in Fig. 3 for most of the coda window at large distances.

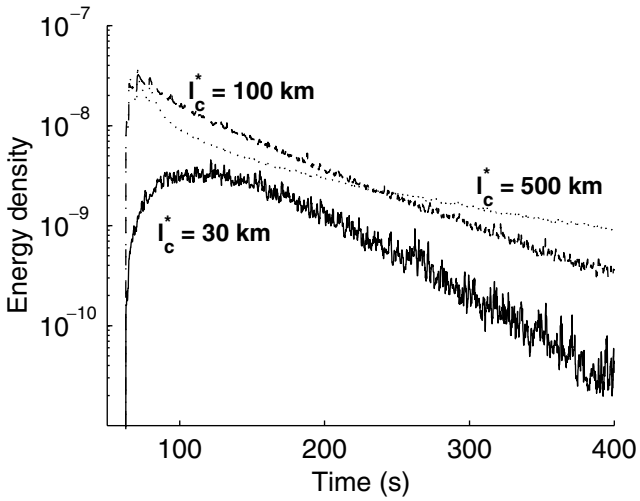

Figure 6. Synthetic coda envelope curves obtained with Monte Carlo simulations for different values of mean free path contrast between crust and mantle. The station is located 220 km away from the source. The mantle transport mean free path is 100 000 km and the crustal transport mean free path is 30 km (solid line), 100 km (dashed line) or 500 km (dotted line).

Early *Lg* coda

To better constrain the model, we now focus on the early *Lg* coda, when energy depends on both time and epicentral distance. Here we apply the principles of MLTWA to regional records dominated by waves trapped in the crust. The time window of comparison between observations and simulations starts when the group velocity becomes smaller than 2.6 km s^{-1} and ends when all energy curves exhibit a steady decay, that is at t = 300 s (Fig. 3). Fig. 8 shows maps of ϵ for both events considered simultaneously. The left-hand side of Fig. 8 shows that acceptable models lie in a narrower band than for the entire coda window (Fig. 7). Moreover, the location of the absolute minimum misfit (right-hand side of Fig. 8) is well defined and remains fairly stable for different normalization windows. A single model with a crustal mean free path of ∼250 km and an absorption length of ∼150 km explains both the space and time attenuation characteristics of the early *Lg* coda in France. Fig. 7 shows that this model also explains the attenuation characteristics of the whole *Lg* coda window.

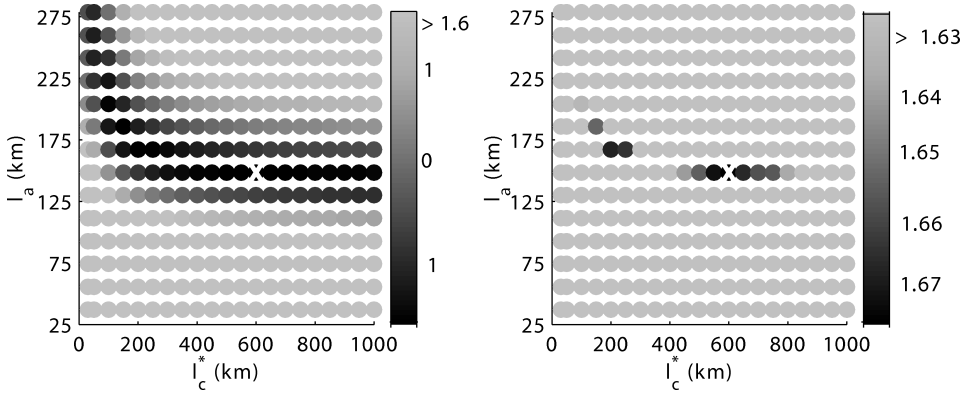

Figure 7. Maps of the misfit value between simulations and observations (ϵ) calculated for the whole *Lg* coda time window at 3 Hz using both earthquakes simultaneously and the normalization window 325–375 s. In the left-hand side, the grey-scale covers the whole amplitude range, while, in the right-hand side, the scale zooms in the narrow amplitude range between the minimum value of ϵ, ϵ_m and $\epsilon_m + 3$ per cent. White crosses indicate locations of the absolute minimum misfit.

Attenuation of the direct *Lg* wave train

We compare our results with those of Campillo *et al.* (1985) and Campillo & Plantet (1991) who measured the quality factor for the direct *Lg* waves in France and found that

$$Q_{Lg}(f) = Q_0 f^{0.52\pm0.1}, \tag{2}$$

with $Q_0 = 290 \pm 80$.

The quality factor of *Lg* can be written as

$$\frac{1}{Q_{Lg}} = \frac{1}{Q_{\rm int}} + \frac{1}{Q_{\rm scat}}, \tag{3}$$

giving a relationship between l_c^* and l_a that is represented as a solid line in Fig. 8 for a frequency of 3 Hz. Models associated with small values of ϵ and close to the solid line explain simultaneously the measured attenuations of the direct waves and *Lg* coda. As a result of the uncertainty on Q_{Lg}, the range of acceptable parameters is still broad as illustrated by Fig. 8. Nevertheless, our preferred model with $l_a = 150$ km and $l_c^* = 250$ km corresponds both to the absolute minimum of the misfit ϵ and to the most probable value of Q_{Lg}. To prove the quality of the fit between synthetics and observations, Fig. 10 compares observed (solid lines) and simulated (dashed lines) coda envelopes for $l_a = 150$ km and $l_c^* = 250$ km for the Saint-Gaudens event. This model correctly agrees with observations in the considered time window (vertical dotted lines) at most stations for the early as well as for the late *Lg* coda. As numerical simulations do not include the direct wave train, a comparison between data and observations cannot be made for this part of the signal.

We have shown that a simple model with only two free parameters ($l_a \sim 150$ km, i.e. $Q_a \sim 800$ and $l_c^* \sim 250$, i.e. $Q_{\rm scat} \sim 1300$) explains the attenuations of the direct *Lg* wave and of the *Lg* coda with both time and distance. However, because of the uncertainty documented by Fig. 8, we cannot conclude which attenuation process is dominant: intrinsic absorption and scattering attenuation are of the same order with respect to the uncertainties. Coda-Q has also been computed, showing that Q_c is 795 ± 25 at 3 Hz, a value close to the estimation of Q_a in our preferred model. This result is in agreement with the model of Margerin *et al.* (1998), which predicts that when l_c^* is much larger than the crustal thickness, the leakage of diffuse energy into the mantle becomes weak. Thereafter, Q_c is in this case essentially a measure of anelastic attenuation. Campillo & Plantet (1991) measured $Q_{\rm scat}$ in France for *Lg* waves, assuming that $Q_{\rm int}$ is ~1500 and is frequency independent. They obtained that $Q_{\rm scat}$ is ~1000 at 3 Hz, in agreement with the measurement made in the present study.

DISCUSSION

Results at other frequencies

Fig. 11 shows maps of the misfit obtained for the two earthquakes considered simultaneously, in the early *Lg* coda time window and for frequency bands centred on 2 Hz (left) and 5 Hz (right). If we

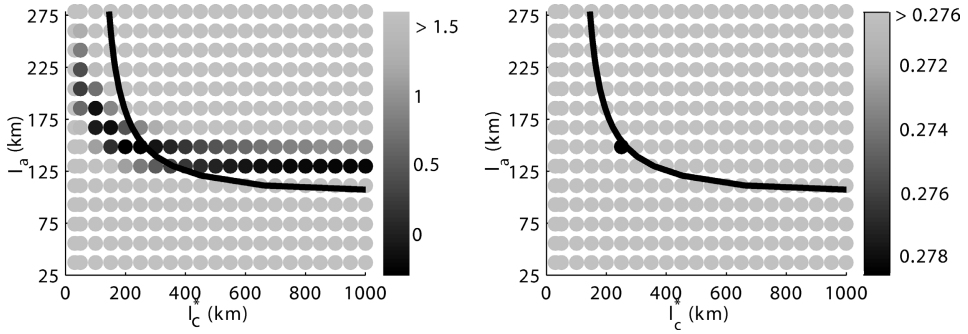

Figure 8. Maps of the misfit value between simulations and observations for the early *Lg* coda time window at 3 Hz. Same legend as Fig. 7. The solid line computed from eq. (3) delineates the set of couples (l_a, l_c^*), which explain *Lg* attenuation as measured by Campillo *et al.* (1985).

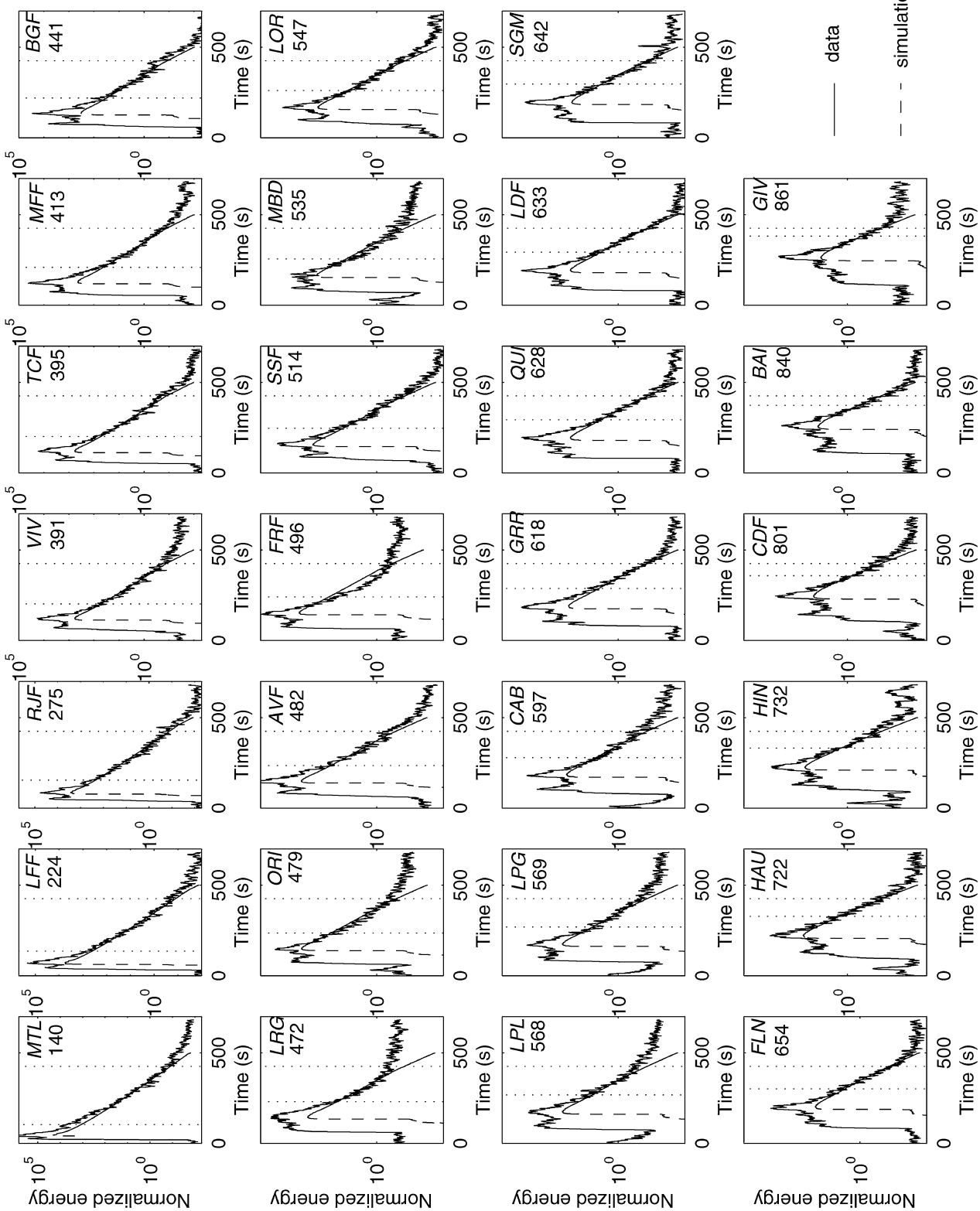

Figure 9. Comparison between observations and simulations for the Saint-Gaudens earthquake at 3 Hz. Solid lines are observed normalized energy curves and dashed lines are synthetic normalized energy curves computed with $l_c^* = 250$ km, $l_m^* = 100\,000$ km and $l_a = 150$ km. The vertical dotted lines delineate the comparison time windows. The station name and epicentral distance are indicated in each panel.

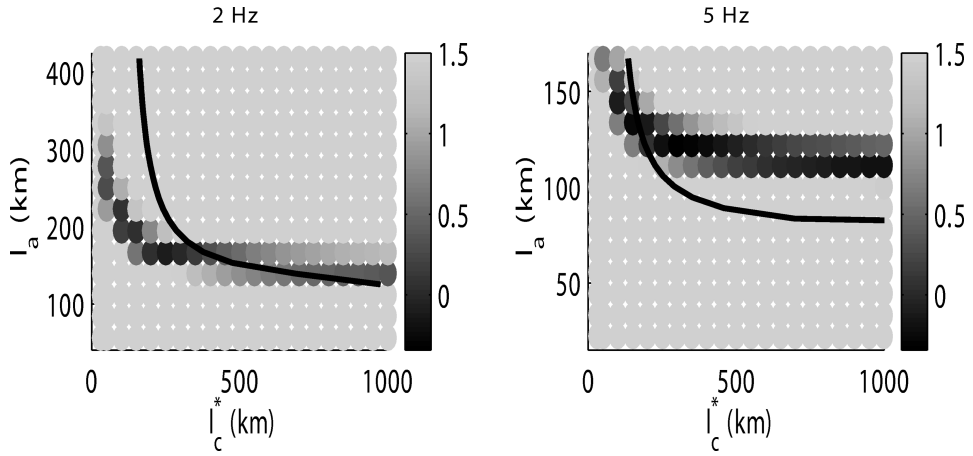

Figure 10. Maps of the misfit value between simulations and observations computed for the early *Lg* coda time window in different frequency bands (left, 2 Hz; right, 5 Hz). The grey-scale covers the entire amplitude range. Solid lines are computed as for Fig. 8.

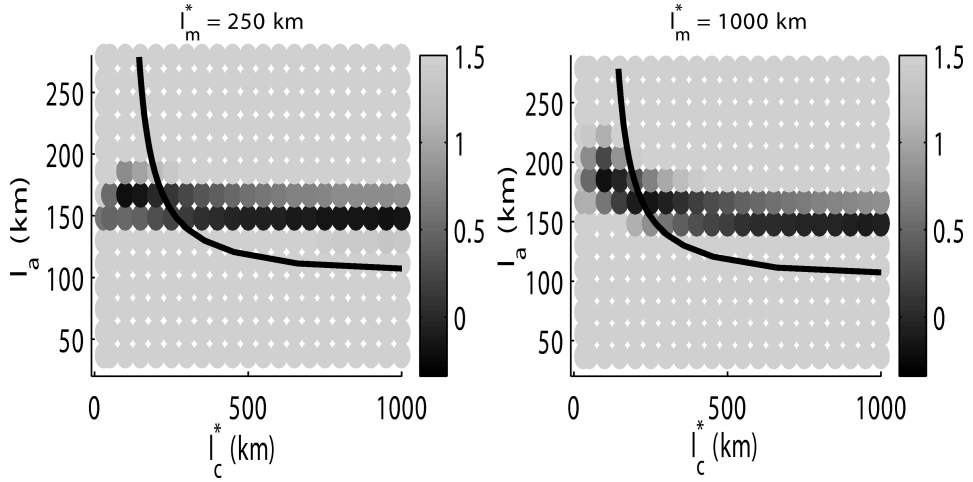

Figure 11. Maps of the misfit value between simulations and observations for the early *Lg* coda time window and different levels of mantle heterogeneity (left, $l_m^* = 250$ km; right, $l_m^* = 1000$ km). Same legend as Fig. 10.

define a reasonable model as the intersection of the band of low ϵ and the curve Q_{Lg}, we find that l_c^* is ∼300 km at 2 Hz and ∼150 km at 5 Hz. Considering the value obtained at 3 Hz (∼250 km), l_c^* appears to depend on frequency. In contrast, l_a is nearly independent of frequency (l_a(2 Hz) ∼ 170 km, l_a(3 Hz) ∼ 150 km and l_a(5 Hz) ∼ 140 km). Because of the uncertainties on the parameters, a detailed discussion on the frequency dependence is impossible.

Influence of mantle heterogeneity

In the previous sections we only considered models with a transparent mantle ($l_m^* = 100\,000$ km). We now check the influence of mantle heterogeneity by assuming weaker values of l_m^*: 250 and 1000 km. The misfit function is computed at 3 Hz for the early *Lg* coda time window, but results and conclusions are the same for other frequency bands (Fig. 11). The level of heterogeneity in the mantle has a negligible effect on the measurement of l_a and l_c^*. This illustrates the dominant part played by crustal guided waves in the build-up of the coda at regional distances. Similar conclusions are reached for the other frequency bands (2 and 5 Hz).

CONCLUSION

A simple stratified model with only two free parameters, the absorption length l_a and the crustal transport mean free path l_c^*, explains the complete envelope of *Lg* waves at regional distances, from the direct *Lg* to the late coda. The best-fitting model is better constrained using the early coda, for which the decay depends on distance, than using the late diffuse coda. This result is in agreement with the technique proposed by Hoshiba (1991) to separate Q_{int} from Q_{scat} using local earthquakes. Our preferred model is characterized by $l_c^* \simeq 250$ km and $l_a \simeq 150$ km at 3 Hz. The trade-off between the two parameters is nevertheless too strong to conclude reliably on the dominance of intrinsic or scattering attenuation, which are qualitatively of the same order of magnitude. Because of the predominance of crustal guided waves at regional distances, the envelope decay is weakly influenced by the level of mantle heterogeneity.

ACKNOWLEDGMENTS

We thank N. Trégourès, B. A. van Tiggelen and R. Hennino for many helpful discussions, and B. Feignier and the Laboratoire de

Géophysique (LDG/CEA) for providing the data. All the computations presented in this paper were performed on the Service Commun de Calcul Intensif de l'Observatoire de Grenoble (SCCI).

REFERENCES

Abubakirov, I.R. & Gusev, A.A., 1990. Estimation of scattering properties of lithosphere of Kamchatka based on Monte Carlo simulation of record envelope of a near earthquake, *Phys. Earth planet. Inter.,* **64,** 52–67.

Aki, K., 1969. Analysis of the seismic coda of local earthquake as scattered waves, *J. geophys. Res.,* **74,** 615–631.

Aki, K., 1980. Attenuation of shear-waves in the lithosphere for frequencies from 0.05 to 25 Hz, *Phys. Earth planet. Inter.,* **21,** 50–60.

Aki, K. & Chouet, B., 1975. Origin of coda waves: source, attenuation and scattering effects, *J. geophys. Res.,* **80,** 3322–3342.

Bois, C., Cazes, M., Hirn, A., Mascle, A., Matte, P., Montadert, L. & Pinet, B., 1988. Contribution of deep seismic profiling to the knowledge of the lower crust in France and neighbouring area, *Tectonophysics,* **145,** 253–275.

Campillo, M. & Paul, A., 1992. Influence of the lower crustal structure on the early coda of regional seismograms, *J. geophys. Res.,* **97,** 3405–3416.

Campillo, M. & Plantet, J.-L., 1991. Frequency dependence and spatial distribution of seismic attenuation in France: experimental results and possible interpretations, *Phys. Earth planet. Inter.,* **67,** 48–64.

Campillo, M., Plantet, J.-L. & Bouchon, M., 1985. Frequency dependent attenuation in the crust neneath central France from *Lg* waves: data analysis and numerical modeling, *Bull. seism. Soc. Am.,* **75,** 1395–1411.

Campillo, M., Feignier, B., Bouchon, M. & Bethoux, N., 1993. Attenuation of crustal waves across the Alpine range, *J. geophys. Res.,* **98,** 1987–1996.

Chandrasekhar, S., 1960. *Radiative Transfer,* Dover, New York.

Chazalon, A., Campillo, M., Gibson, R. & Carreno, E., 1993. Crustal wave propagation anomaly across the Pyrenean Range. Comparison between observations and numerical simulations, *Geophys. J. Int.,* **115,** 829–838.

Dainty, A.M. & Toksöz, M.N., 1990. Array analysis of seismic scattering, *Bull. seism. Soc. Am.,* **80,** 2242–2260.

Fehler, M., Hoshiba, M., Sato, H. & Obara, K., 1992. Separation of scattering and intrinsic attenuation for the Kanto-Tokai region, Japan, using measurement of *S*-wave energy versus hypocentral distance, *Geophys. J. Int.,* **108,** 787–800.

Fuchs, K., Bonjer, K.P., Gajewski, D., Lüschen, E., Prodehl, C., Sandmeier, K.J., Wenzel, F. & Wilhelm, H., 1987. Crustal evolution of the Rhinegraben area. 1. Exploring the lower crust in the Rhinegraben rift by unified geophysical experiments, *Tectonophysics,* **141,** 261–275.

Gusev, A., 1995. Vertical profile of turbidity and coda *Q*, *Geophys. J. Int.,* **123,** 665–672.

Hoshiba, M., 1991. Simulation of multiple scattered coda wave excitation based on the energy conservation law, *Phys. Earth planet. Inter.,* **67,** 123–136.

Hoshiba, M., 1993. Separation of scattering attenuation and intrinsic absorption in Japan using the multiple lapse time window analysis of full seismogram envelope, *J. geophys. Res.,* **98,** 15 809–15 824.

Hoshiba, M., 1994. Simulation of coda wave envelope in depth dependent scattering and absorption structure, *Geophys. Res. Lett.,* **21,** 2853–2856.

Hoshiba, M., 1997. Seismic coda wave envelope in depth dependent *S*-wave velocity structure, *Phys. Earth planet. Inter.,* **104,** 15–22.

Hoshiba, M., Rietbrock, R., Scherbaum, F., Nakahara, H. & Haberland, C., 2001. Scattering attenuation and intrinsic absorption using unifrom and depth dependent model—application to full seismogram envelope recorded in Northern Chile. *J. Seismol.,* **5,** 157–179.

Jin, A., Mayeda, K., Adams, D. & Aki, K., 1994. Separation of intrinsic and scattering attenuation in southern California using TERRAscope data, *J. geophys. Res.,* **99,** 17 835–17 848.

Kourganoff, V., 1963. *Basic Methods in Transfer Problems: Radiative Equilibrum and Neutron Diffusion,* Dover, New York.

Lux, I. & Koblinger, L., 1991. *Monte Carlo Particle Transport Methods: Neutron and Photon Calculations,* CRC Press, Boca Raton.

Margerin, L., Campillo, M. & Van Tiggelen, B.A., 1998. Radiative transfer and diffusion of waves in a layered medium: new insight into coda *Q*, *Geophys. J. Int.,* **134,** 596–612.

Margerin, L., Campillo, M., Shapiro, N.M. & Van Tiggelen, B.A., 1999. Residence time of diffuse waves in the crust as a physical interpretation of coda *Q*: application to seismograms recorded in Mexico, *Geophys. J. Int.,* **138,** 343–352.

Mayeda, K., Su, F. & Aki, K., 1991. Seismic albedo from the total seismic energy dependence on hypocentral distance in southern California, *Phys. Earth planet. Inter.,* **67,** 104–114.

Mayeda, K., Koyanagi, S., Hoshiba, M., Aki, K. & Zeng, Y., 1992. A comparative study of scattering, intrinsic and coda Q^{-1} for Hawaii, Long Valley and Central California between 1.5 and 15 Hz, *J. geophys. Res.,* **97,** 6643–6659.

Nicolas, M., Massinon, B., Mechler, P. & Bouchon, M., 1982. Attenuation of regional phases in Western Europe, *Bull. seism. Soc. Am.,* **72,** 2089–2106.

Perrier, G. & Ruegg, J.C., 1973. Structure profonde du Massif Central Français, *Ann. Geophys.,* **29,** 435–502.

Rytov, S.M., Kravtsov, Y.A. & Tatarskii, V.I., 1989. 4. Wave propagation through random media, in *Principle of Statistical Radiophysics,* Springer-Verlag, Berlin.

Ryzhik, L., Papanicolaou, G. & Keller, J.B., 1996. Transport equations for elastic and other waves in random media, *Wave motion,* **24,** 327–370.

Sato, H. & Fehler, M., 1998. *Wave propagation and scattering in the heterogeneous Earth,* Springer-Verlag, New York.

Sato, H., Nakahara, H. & Ohtake, M., 1997. Synthesis of scattered energy density for nonspherical radiation from a point shear-dislocation source based on the radiative transfer theory, *Phys. Earth planet. Inter.,* **104,** 1–13.

Ugalde, A., Pujades, L.G., Canas, J.A. & Villaseñor, A., 1998. Estimation of the intrinsic absorption and scattering attenuation in Northeastern Venezuela (Southeastern Caribbean) using coda waves, *Pure appl. Geophys.,* **153,** 685–702.

Wu, R.S., 1985. Multiple scattering and energy transfer of seismic waves-separation of scattering effect from intrinsic attenuation—I. Theoretical modelling, *Geophys. J. R. astr. Soc.,* **82,** 57–80.

Wu, R.S. & Aki, K., 1988. Multiple scattering and energy transfer of seismic waves-Separation of scattering effect from intrinsic attenuation—II. Application of the theory to Hindu Kush Region, *Pure appl. Geophys.,* **128,** 49–80.

Wu, R.S. & Aki, K., 1988. Introduction to the wave scattering in three-dimensionnally heterogeneous Earth, *Pure appl. Geophys.,* **128,** 1–6.

Zeng, Y., Su, F. & Aki, K., 1991. Scattering wave energy propagation in a random isotropic scattering medium 1. Theory, *J. geophys. Res.,* **96,** 607–619.